CrystEngComm

Accepted Manuscript

ROYAL SOCIETY OF CHEMISTRY

www.rsc.org/crystengcomm

Journal Name

RSCPublishing

ARTICLE

Up-conversion luminescence properties of lanthanide-doped LuF3 with different morphologies synthesized via a facile ionothermal process

Cite this: DOI: 10.1039/xoxxooooox

Received ooth January 2012,
Accepted ooth January 2012

DOI: 10.1039/xoxxooooox

www.rsc.org/

Xue Yu, [a,b] Wenjuan Bian, [a] Ting Wang, [a] Dacheng Zhou, [a,b] Jianbei Qiu [a,b,*] and Xuhui Xu [a,b,*]

Up-conversion (UC) crystals of lanthanide-doped LuF_3 with different morphologies (nanoparticles, shuttle and litchi-like microcrystals) have been synthesized via a facile ionothermal method. The dependence of the morphological differences of the products on the solvent composition and reaction time has been studied in detail, and a possible formation mechanism has also been proposed. The emission spectra showed that the UC luminescence intensity can be adjusted by changing the morphology of LuF_3. Both LuF_3:Yb^{3+}/Er^{3+} and LuF_3:Yb^{3+}/Ho^{3+} nanoparticles synthesized using water/IL (ionic liquid) as mixed solvent exhibit a significant enhancement of the yellowish-green emission under 980nm laser excitation. Besides, nearly NIR (near-infrared) to NIR UC luminescence has been achieved in LuF_3:Yb^{3+}/Tm^{3+} nanoparticles synthesized using EG (ethylene glycol)/IL as mixed solvent. Furthermore, the ratio of the emission intensity of 812nm to that of 545nm reaches 55. Our results indicate that lanthanide-doped LuF_3 provide a promising application in chromatic displays and bio-imaging.

1. Introduction

The lanthanide-doped UC nanoparticles (NPs) show superior features including long emission lifetimes, high photochemical stability, low toxicity, and high penetration depth, making them highly suitable for use as alternatives to organic fluorescent dyes or quantum dots for various bioapplications such as early cancer theranostics.[1] And crucially, UCNPs are well known due to their unique energy UC luminescence capabilities, which could emits high-energy photons followed by the effective absorption of low-energy photons. UCNPs usually exhibit novel luminescence properties, depending on their structure, shape, and size, such as tunable wavelengths, rapid responsibilities, and high efficiencies.[2] Thus, it is extremely important in nanotechnique and nanoscience to develop synthesis methods with well-shaped UCNPs.

In the search of practically available UC materials, it is already known that host matrix effects are essential for UC transitions of lanthanide ions and thus contributes to the controllable emission bands and high efficiency. It is well-known that fluorides offer multiple advantages as host matrices for lanthanide ions, as they are typically characterized by a high transparency, a wide band gap, and low energy phonons minimizing multi-phonon relaxation.[3] Moreover, the optical behavior is strongly influenced by the impurities and defects in the crystal lattice. Thus, the searching of oxygen-free hosts is indispensable and will greatly boost the development of high efficiency UC phosphors in various applications for the fact that the oxide UCNPs generally suffer from low emission efficiency due to structural defects (e.g. oxygen vacancy). The binary lanthanide fluoride was found to be a promising host lattice due to its low phonon energy leading to a minimization of the excited states quenching. It gives rise to a long luminescent lifetime and high luminescent quantum yields. More importantly, the ease of substitution of the rare earth (Re) ions by other Re ions with the same valence, and the small particles size of the Re fluoride make it appealing to biological applications.

Unfortunately, the preparation of binary lanthanide fluoride (LnF_3) nanoparticles is not easy and only a few reports have appeared so far. Well-established methods for preparing LnF_3 nanoparticles are hydrothermal,[4] sonochemistry-assisted,[5] microemulsion[6] and sol-gel[7] synthesis routes. However, these methods have several disadvantages such as (1) the use of surfactants or templates may introduce heterogeneous impurities in the products, (2) severe experimental conditions or complicated and time-consuming post-treatments increases the production cost.[8] Therefore, it is required to develop a more facile and reproducible procedure to synthesize LnF_3 nanoparticles with high crystallinity.

Ionothermal synthesis is a kind of thermal reaction that uses ionic liquids (ILs), which have emerged as exceptionally interesting reaction media for enzymatic transformations because of their unique solvent properties, headed by their negligible vapour pressure and their exceptional ability to maintain enzymes in active and stable conformations.[9] Task-specific ionic liquids offer the advantage that they can be used both as solvent and reactant, which decrease the number of reaction parameters. Among the various kinds of ILs, 1-butyl-3-methylimidazolium tetrafluoroborate , $BmimBF_4$, is one of the most commonly used ILs which can be used for the synthesis of metal fluorides by utilizing the F^- ions released by BF_4^- anions in ILs under the appropriate conditions.[10] The aim of the work presented here is to optimize this fast and facile synthesis route for the fabrication of pure, oxygen-free fluoride nanophosphors.

Herein, lanthanide-doped LuF_3 UC crystals with different morphologies (nanoparticles, shuttle-like and litchi-like microcrystals) have been synthesized by using $BminBF_4$ as reaction medium and fluoride source. In order to explore the effects of the solvent composition on the formation and optical performance of the final product, a contrast experiments have been performed using ethyleneglycol (EG) as a substitute for water. In addition, the effects of reaction time on the size and morphology of the products have been studied in detail, and a possible formation mechanism has also been proposed. The uniform self-assembling morphology and bright UC luminescence indicates this material is a promising candidate for chromatic displays and bio-imaging.

2. Experimental

LuF_3 nanocrystals (NCs) doped with $Yb^{3+}/Tm^{3+}/Ho^{3+}$ were synthesized via an ionothermal method using ILs and deionized water/EG as the solvent mixture. Select the synthesis of LuF_3: 15% Yb^{3+}, 1% Tm^{3+}, 1% Ho^{3+} as an example. Firstly, Lu_2O_3 (Aldrich, 99.99%), Yb_2O_3 (Aldrich, 99.99%), Tm_2O_3 (Aldrich, 99.99%), Er_2O_3 (Aldrich, 99.99%), Eu_2O_3 (Aldrich, 99.99%), and Ho_2O_3 (Aldrich, 99.99%) were added to a beaker containing moderate concentrated nitric acid (HNO_3) and then heated at 90°C and stirred with glass rod until formed corresponding nitrate solution and evaporated extra concentrated nitric acid. Then 1-butyl-3-methylimidazolium tetrafluoroborate ($BmimBF_4$) and moderate deionized water were added into the above beaker and the pH were kept to be 5. Afterwards, the above mixed solution were stirred for 30 min at room temperature and then transferred into a 50 ml Teflon-lined autoclave and kept at 180°C for 1h/4h. The system was then allowed to cool down to room temperature and the final products deposited at the bottom of the vessel. The nanocrystals were separated via centrifugation and washed two times with deionized water and finally once with ethanol. The products were obtained as a white powder after drying at 80°C in a baking oven.

X-Ray powder diffraction (XRD) was performed using a D8 Focus diffractometer (Bruker) with Cu Kα radiation (λ= 0.15405 nm) in the 2θ range from 20° to 80°. The particle morphology and size were studied with field transmission electron microscopy (TEM) and high-resolution field transmission electron microscope (HRTEM), carried out using U.S. FEI Tecnai G2 F20 operating at 200 kV. The TEM and selected area electron diffraction (SAED) images were recorded to provide more information about the structure of LuF_3. The energy-dispersive X-ray (EDX) elemental mapping images were recorded on a Hitachi S-3500N scanning electron microscope, operated at 200 kV and a resolution of 102 eV. The UC luminescence spectra of the samples under a 980 nm infrared laser excitation were recorded by HITACHIU-F-7000 spectrophotometer at room temperature.

3. Results and discussion

The density functional theory calculations of LuF_3 based on the crystal structure refinement are shown in Fig.1. The local density approximation (LDA) was chosen for the theoretical basis of the density function. From sampling the number of electronic states in k space at the each energy, one can determine the atomic position of LuF_3, and then calculate their band structures, as displayed in Fig.1A. It could be determined that orthorhombic LuF_3 possessed a direct band-gap of about 6.350 eV with the valence band (VB) maximum at the G point of the Brillouin zone (inset of Fig. 1B). Fig. 1B, C and D show total density of states (TDOS) and atomic partial DOS (Lu, F) of the sample. It could be concluded the conduction band (CB) of LuF_3 consist of Lu 4f orbitals and F 2p orbitals, whereas the VB is dominated by Lu 4d orbitals. It is expected that the value of the calculated band-gap of LuF_3 will be smaller than the experimental one as the LDA underestimates the size of the band-gap.[11]

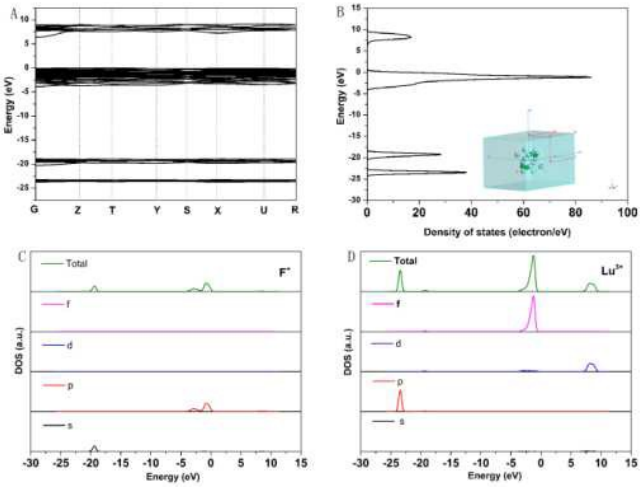

Figure 1 (A) band structure; (B) density of states; Inset: Brillouin zone; (C) total and partial density of states of F^-; (D) total and partial density of states of Lu^{3+}.

The phase characteristics of the products by the ionothermal treatment with different solvent compositions for 1h were examined by XRD, as shown in Fig. 2. All diffraction peaks of the samples match well with the standard data of the

orthorhombic phase LuF_3 (JCPDS No. 32-0612). No traces of impurity peaks were detected, which indicates that a single phase of LuF_3 could be obtained. The average crystallite size of the product can be estimated from the Scherrer formula, $D=K\lambda/\beta\cos\theta$, where D is the average particle size, λ is the X-ray wavelength (0.15405nm), β is the full-width at half-maximum, θ is the diffraction angle of an observed peak, and K is a constant (0.89), respectively. For the samples obtained from different solvent compositions (IL/water and IL/EG), the estimated average crystallite sizes were calculated to be 38.5 and 42.4 nm, respectively.[12]

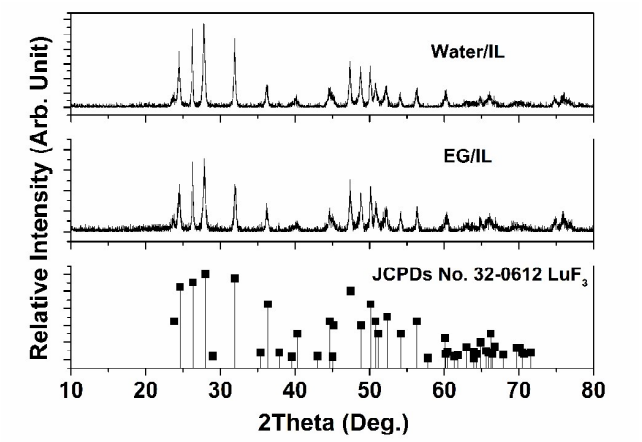

Figure 2 XRD patterns of LuF_3 synthesized using water/IL and EG/IL as mixed solvent, respectively.

As shown in Fig.3 A and B, the morphology and particle size of the as-prepared samples were examined using TEM. The sample synthesized in IL/water exhibits an irregular shape consisting of spherical and elliptical particles with an average size around 40 nm, while nanocrystals prepared in IL/EG have a nearly uniform elliptical shape with a length of 45 nm and a diameter of 25 nm, which are in good agreement with the results of XRD. The crystal structure of individual nanoparticle is further characterized by the SAED (inset of Fig. 3A and B) and HRTEM (inset of Fig. 3a and b). The corresponding SAED patterns, taken from both samples, show the diffraction rings, indicating that both the as-prepared samples are polycrystalline. The concentric rings from inside to outside could be indexed to the specific (111) and (131) planes of LuF_3 lattice, respectively, confirming the successful preparation. The inset of Fig. 3a and b display typical HRTEM images of the polycrystalline nanoparticles, and the distance between the lattice fringes was measured to be about 0.35 nm, which corresponds to the *d*-spacing for the (101) lattice plane of the orthorhombic LuF_3 structure, confirming the high crystallinity of the products. Generally speaking, high crystallinity is important for luminescent materials because high crystallinity means fewer traps and stronger luminescence intensity.[13]

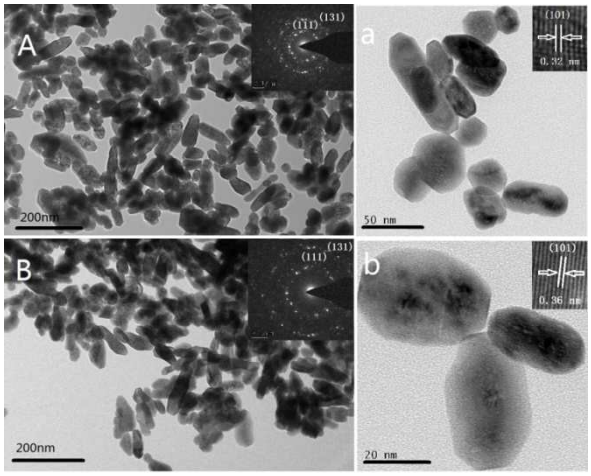

Figure 3 TEMs (A), SAED (Inset of (A)), enlarged TEMs (a), and HRTEM of LuF_3 nanocrystals prepared with water/IL solvent; TEMs (B), SAED (Inset of (B)), enlarged TEMs (b), and HRTEM of LuF_3 nanocrystals prepared with EG/IL solvent.

The excitation and emission spectra of LuF_3:Eu^{3+} prepared with IL/water (solid line) and IL/EG (dash line) were shown in Fig.4. LuF_3:Eu^{3+} samples exhibits similar photoluminescence properties with different emission intensity. Monitoring the emission at 592 nm (the $^5D_0\rightarrow{}^7F_1$ transition of Eu^{3+} ions), the excitation spectra of these two samples consist of the characteristic excitation lines of Eu^{3+} within its $^4f_6$ configuration from 200 to 500 nm. The strongest excitation peak at 393nm is assigned to the $^7F_0\rightarrow{}^5L_6$ transition of Eu^{3+}. It is well know that in the Eu-doped systems, charge transfer occurs by electron delocalization from the filled 2p shell of ligand to the partially filled 4f shell of Eu^{3+}. The transition energy depends strongly on the electronegativity of the ligand. For Eu^{3+} in oxide hosts, a charge transfer band (CTB) of Eu^{3+}-O^{2-} is frequently observed between 200 and 300 nm in the excitation spectra. Owing to the high electronegativity of the pure fluoride compounds, much higher energy is needed to remove an electron from F^- than from O^{2-}, consequently the CTB of Eu^{3+}-F^- is generally located below 200 nm.[9b] The absence of CTB (Eu^{3+}-O^{2-}) in UV region further confirms that oxygen-free LuF_3 host is successfully synthesized. Under the excitation of 393 nm, the emission peaks centered at 510, 555, 592, 617 651 and 696 nm were observed, which could be contributed to the transitions of $^5D_2\rightarrow{}^7F_3$, $^5D_1\rightarrow{}^7F_2$, $^5D_0\rightarrow{}^7F_1$, $^5D_0\rightarrow{}^7F_2$, $^5D_0\rightarrow{}^7F_3$ and $^5D_0\rightarrow{}^7F_4$, respectively.[14] The emission at 617 nm belongs to a hypersensitive forced electro-dipole transition, which depends on the symmetries of the local environment around Eu^{3+} ions, and it is permitted only at the low symmetry without inversion center.[8] The emission at 592 nm is from a magnetic-dipole transition which is insensitive to the local symmetry. It is worth noting that the intensity of 592 nm is stronger than that of 617 nm, which demonstrates the formation of the centro-symmetrical structure of lutetium fluoride.[15] Besides, although the emission positions of the two samples are identical, the emission intensity of IL/water sample

is much higher than that of IL/EG sample. Generally speaking, such differences in the PL spectra can be caused by factors like the extent of crystallinity, morphology, size distribution, homogeneity, and dimension of the phosphor. XRD results revealed that these two samples with different solvent compositions are highly crystallized with the same crystal structure and similar crystallization degree. Therefore, the difference in the emission intensity could be derives from the different morphologies and dimensions, implies the optical behavior is strongly dependent on the morphology and dimension of these product.

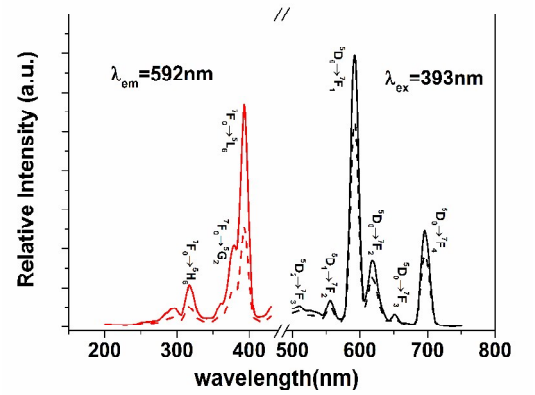

Figure 4 Excitation and emission spectra of LuF_3:Eu^{3+} synthesized using water/IL and EG/IL as mixed solvent, respectively.

The reaction time has been demonstrated to be a key parameter for controlling the shape and size of the products.[10] Therefore, to further investigate the influence of morphology and size on the optical property of the products, we take LuF_3:Yb^{3+}/Tm^{3+} as a representative example to conduct the time-dependent experiments using water and EG as solvent composition, respectively. A noticeable result could be found that the crystal structure and morphology of LuF_3 nanoparticles have not obviously changed after doping with different Re ions (Yb^{3+}, Er^{3+}, Ho^{3+}, or Tm^{3+}). SEM images of the products with increased reaction time (4h) are given in Fig. 5. It is interesting to see that, the products of LuF_3:Yb^{3+}/Tm^{3+} formed in different solvent environments show the regular morphologies, which are assembled by a lot of nanoparticles. When using IL and water as mixed solvent, a great amount of shuttle-like superstructures was obtained in the product along with little chain-shaped superstructures. While nearly monodisperse and regular litchi-like particles can be obtained when water was replaced with EG as solvent. Both the structural features can be identified clearly in the enlarged TEM image, as shown in the inset of Fig. 5a and b. The magnified image showed that shuttle-like submicron particles consisting of spherical and elliptical nanoparticles. The wide of the submicron particles is estimated to be about 80 nm, while the length ranges from 140 to 180 nm. For IL/EG sample, nearly all of the obtained particles possess similar morphology with the diameter about 140 nm, which is composed of numerous aggregated elliptical shape nanocrystallites. The bottom of Fig. 5 represents the mappings of fluorine, lutecium, ytterbium and thulium elements in both samples, respectively. It can be seen that all of the elements are well-distributed inside these particles, revealing the uniform chemical phase.

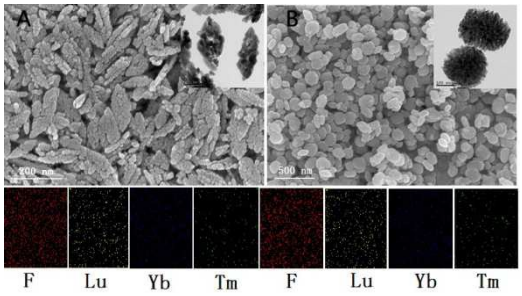

Figure 5 SEMs (A and B) and TEMs (inset) of LuF_3:Yb^{3+},Tm^{3+} synthesized using water/IL and EG/IL with a 4h reaction time. The bottom is the corresponding mappings of F, Lu, Yb and Tm elements.

On the basis of the experimental results, a possible formation mechanism is proposed as shown in Fig 6. As the reaction time is prolonged, many small nanoparticles with identical crystal orientation will spontaneously organize together followed by attachment to each other on an identical plane according to a certain direction, which leads to the decrease in the whole surface energy so as to maintain the condition of lowest energy. Both processes could be related to a proposed mechanism of the so-called "orientated attachment" by Penn and Banfield and co-workers.[16] For IL/Water sample, the nano-chains could be formed as the primary nanoparticles grow,, and then shuttle-like submicron particles could be obtained after further growth, which finally forms a complex structure. The different morphologies observed in samples from IL/EG as solvent may be attributed to the different viscosities of the solvent mixture, which have great influence to the nucleation and crystal growth processes.

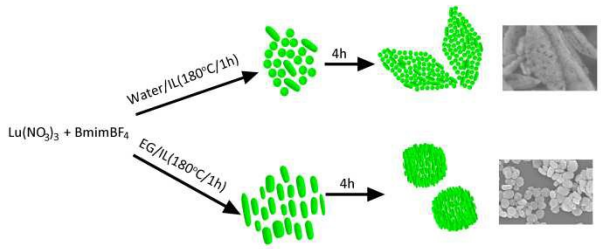

Figure 6 Schematic illustration of the growth processes of LuF_3 microcrystals.

Fig. 7 displays the UC emission spectra of Yb^{3+}/Ln^{3+} (Ln=Ho, Er, Tm) codoped LuF_3 samples with IL/Water (a, b, c) and IL/EG (A, B, C) under 980 nm laser excitation, respectively. It is clear to see that the bright yellowish-green emission can be detected in both LuF_3:Yb^{3+}/Er^{3+} and LuF_3:Yb^{3+}/Ho^{3+} samples synthesized in IL/Water solvent. In LuF_3:Yb^{3+}/Er^{3+}, two emission peaks in the visible region

centered at 547 and 661 nm can be assigned to the $^4S_{3/2}\rightarrow{}^4I_{15/2}$ and $^4F_{9/2}\rightarrow{}^4I_{15/2}$ transitions of Er^{3+}, respectively. LuF_3:Yb^{3+}/Ho^{3+} yields a yellowish-green emission which is ascribed to the red emission (645 nm) of $^5F_5\rightarrow{}^5I_8$ and a relative stronger green emission (544nm) of $^5S_2\rightarrow{}^5I_8$ of Ho^{3+}. While in LuF_3:Yb^{3+}/Tm^{3+} synthesized in both IL/Water and IL/EG solvents (Fig. 7 c and C), a series of characteristic emission peaks of the Tm^{3+} ions ranging from visible blue to NIR are clearly observed, with the dominant emission at 812 nm. Although the major peaks in the emission spectra are identical in all samples, the intensities of the emission peaks increase with increasing reaction time. Here, two mechanisms might cause the enhancement of UC emissions intensity. (1) It is well known that the crystallinity of products is improved with increasing reaction time, which is favorable to improve the luminescent intensity. (2) The oriented aggregation of nanophosphors could significantly enhance the luminescent emissions at nanoscale. Surface defects generally act as quenching centers, causing the fluorescence from the surface centers quenched.[3] The smaller nanoparticle exhibits weak emission intensity, which is usually ascribed to a larger surface to volume ratio as well as abundant defects on its surface. When the nanoparticles aggregated to be shuttle-like or litchi-like microcrystals, some defects will be sandwiched into the microcrystals, which results in the increase of the emission intensity. Importantly, for LuF_3:Yb^{3+}/Tm^{3+} synthesized in IL/EG solvent, the relative intensity of the NIR to green is enhanced greatly as reaction time is prolonged, and the ratio of the emission at 812 to that of 545 nm reaches 55. These are beneficial to deeper tissue penetration and reduced autofluorescence, because the NIR spectral range (700-1100 nm) is generally addressed as the "optical window" of the biological tissues, due to the lack of efficient endogenous absorbers.[2a] Therefore, LuF_3:Yb^{3+}/Tm^{3+} nanoparticles may find potential applications in the high contrast in vitro and in vivo imaging and bio-separation.

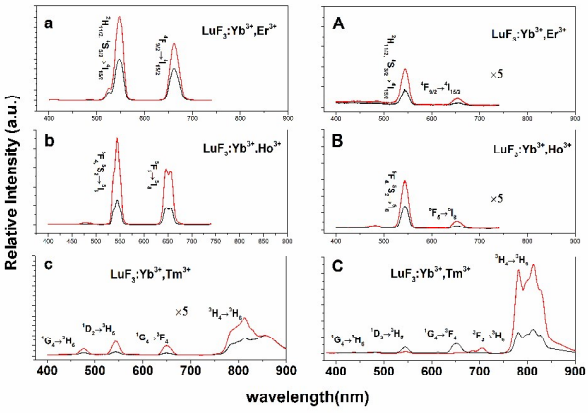

Figure 7 Up-conversion luminescence spectra of LuF_3:Yb^{3+}, Er^{3+}, LuF_3:Yb^{3+},Ho^{3+}, and LuF_3:Yb^{3+},Tm^{3+} under 980 excitation with different reaction time (black line: 1h, red line: 4h).

To further study the photon excitation process, power dependent UC emission spectra of representative samples were performed. As shown in Fig.8, the UC emission intensity (I_{UC}) of these samples increase with increasing excitation power (P), with a power law of IPn, where n represents the number of pumping photons required to excite rare earth ions from the ground state. For LuF_3:Yb^{3+}/Er^{3+} and LuF_3:Yb^{3+}/Ho^{3+}, the slopes are assigned to be 5.2 and 3.9, respectively. The observed slopes for both samples suggest that they all involve a multi-photon process. The band centered at 812nm (NIR) of LuF_3:Yb^{3+}/Tm^{3+} (n=2.2) is dominated by a two-photon upconversion process. The excellent NIR to visible ratio is due to the higher probability of the NIR emission, which is ascribed to the smaller number of phonons required from the LuF_3 host to fill up the energy mismatch. However, it is not an absolute rule, for instance, when photon avalanche or pumping saturation effect happens, the value of n may be also much larger than the photon number, or much smaller than the photon number.[17]

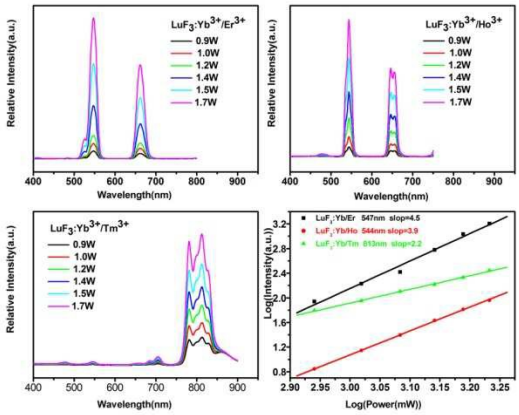

Figure 8 Up-conversion luminescence spectra of LuF_3:Yb^{3+}, Er^{3+}(A), LuF_3:Yb^{3+},Ho^{3+}(B), and LuF_3:Yb^{3+},Tm^{3+} (C) under 980 excitation with different pump power. (D). Power density dependence for the main emissions of LuF_3:Yb^{3+},Ln^{3+} (L=Er, Ho, Tm).

Conclusions

In summary, we successfully synthesized the orthorhombic LuF_3 as a highly promising host material for efficient UC generation for lanthanide ions via a facile ionothermal method. The results reveal that the perfect self-assembling morphology can be obtained in different solvent compositions with the reaction ongoing. Both LuF_3:Yb^{3+}/Er^{3+} and LuF_3:Yb^{3+}/Ho^{3+} nanoparticles synthesized using water/IL(ionic liquid) as mixed solvent exhibit the bright yellowish-green emission under 980 nm laser excitation. Beyond that, nearly NIR (near-infrared) to NIR up-conversion has been achieved in Yb^{3+}/Tm^{3+} incorporated samples. All emission spectra showed that the UC luminescence intensity can be adjusted with changing morphology of LuF_3. It is observed that the intensity of the emission bands remarkable improved with the reaction time increase. Importantly, the relative intensity of the NIR to green is enhanced greatly as the reaction time prolonged in LuF_3:Yb^{3+}/Tm^{3+} samples synthesized in IL/EG solvent, and the ratio of the emission at 812 to that of 545 nm reaches 55.

Lanthanide-doped LuF_3 nanoparticles may find potential uses in high-contrast in vitro and in vivo imaging and bio-separation.

Acknowledgements

Project supported by the National Nature Science Foundation of China (61308091, 11204113), Specialized Research Fund for the Doctoral Program of Higher Education of China (20115314120001).

Notes and references

[a] College of Materials Science and Engineering, Kunming University of Science and Technology, Kunming, 650093, P. R. China
[b] Key Laboratory of Advanced Materials of Yunnan Province, Kunming, 650093, P. R. China
*Corresponding author, E-mail: xuxuh07@126.com, qiu@kmust.edu.cn

1. (a) F. Wang and X. Liu, Recent advances in the chemistry of lanthanide-doped upconversion nanocrystals, *Chem. Soc. Rev.*, 2009, ***38*** (4), 976-989; (b) S. K. Maji, S. Sreejith, J. Joseph, M. Lin, T. He, Y. Tong, H. Sun, S. W. K. Yu and Y. Zhao, Upconversion nanoparticles as a contrast agent for photoacoustic imaging in live mice, *Adv. Mater.,* 2014, ***26*** (32), 5633-5638.
2. (a) S. Zeng, Z. Yi, W. Lu, C. Qian, H. Wang, L. Rao, T. Zeng, H. Liu, H. Liu and B. Fei, Upconversion: Simultaneous Realization of Phase/Size Manipulation, Upconversion Luminescence Enhancement, and Blood Vessel Imaging in Multifunctional Nanoprobes Through Transition Metal Mn^{2+} Doping, *Adv. Funct. Mater.*, 2014, **24** (26), 4196-4196; (b) Y. Liu, D. Tu, H. Zhu and X. Chen, Lanthanide-doped luminescent nanoprobes: controlled synthesis, optical spectroscopy, and bioapplications, *Chem. Soc. Rev.*, 2013, **42** (16), 6924-6958.
3. Y. Tian, J. Tian, X. Li, B. Yu and T. Shi, Facile synthesis of ultrasmall GdF_3 nanowires via an oriented attachment growth and their luminescence properties, *Chem. Comm.,* 2011, **47** (10), 2847-2849.
4. M. Pedroni, F. Piccinelli, T. Passuello, M. Giarola, G. Mariotto, S. Polizzi, M. Bettinelli and A. Speghini, Lanthanide doped upconverting colloidal CaF_2 nanoparticles prepared by a single-step hydrothermal method: toward efficient materials with near infrared-to-near infrared upconversion emission, *Nanoscale*, 2011, **3** (4), 1456-1460.
5. R.-X. Yan and Y. Li, Down/Up Conversion in Ln^{3+}-Doped YF_3 Nanocrystals, *Advanced Functional Materials*, 2005, **15** (5), 763-770.
6. J.-L. Lemyre and A. M. Ritcey, Synthesis of lanthanide fluoride nanoparticles of varying shape and size, *Chem. Mater.*, 2005, **17** (11), 3040-3043.
7. S. Fujihara, S. Koji and T. Kimura, Structure and optical properties of (Gd, Eu)F_3-nanocrystallized sol–gel silica films, *J. Mater. Chem.*, 2004, **14** (8), 1331-1335.
8. C. Lorbeer, J. Cybińska and A.-V. Mudring, Europium (III) fluoride nanoparticles from ionic liquids: structural, morphological, and luminescent properties, *Cryst. Growth Des.*, 2011, **11** (4), 1040-1048.
9. (a) Z. Miao, Z. Liu, K. Ding, B. Han, S. Miao and G. An, Controlled fabrication of rare earth fluoride superstructures via a simple template-free route, *Nanotechnology,* 2007, **18** (12), 125605 (1-5); (b) L. Zhu, X. Liu, J. Meng and X. Cao, Facile sonochemical synthesis of single-crystalline europium fluorine with novel nanostructure, *Cryst. Growth Des.,* 2007, **7** *(*12), 2505-2511.
10. Y. Wu, D. Yang, X. Kang, Y. Zhang, S. Huang, C. Li and J. Lin, Luminescent LaF_3: Yb^{3+}/Er^{3+} crystals with self-assembling microstructures by a facile ionothermal process, *CrystEngComm* **2014,** *16* (6), 1056-1063.
11. L. Guo, Y. Wang, L. Han, Q. Qiang, W. Zeng, Z. Zou, B. Wang and X. Guo, Band structure, shape controllable synthesis and luminescence properties of the precursor and final product $Lu_6O_5F_8$: Eu/Tb/Ce/Dy nano/microstructures, *J. Mater. Chem. C,* 2013, **1** (47), 7952-7962.
12. Y. Sun, H. Liu, X. Wang, X. Kong and H. Zhang, Optical spectroscopy and visible upconversion studies of YVO_4: Er^{3+} nanocrystals synthesized by a hydrothermal process, *Chem. Mater.*, 2006, **18** (11), 2726-2732.
13. G. Y. Hong, B. S. Jeon, Y. K. Yoo, and J. S. Yoo, Photoluminescence characteristics of spherical Y_2O_3: Eu phosphors by aerosol pyrolysis, *J. Electrochem.l Soc.*, 2001, **148** (11), H161-H166.
14. Y. Wang, Y. Liu, Q. Xiao, H. Zhu, R. Li and X. Chen, Eu^{3+} doped KYF_4 nanocrystals: synthesis, electronic structure, and optical properties, *Nanoscale*, 2011, **3** (8), 3164-3169.
15. W. Luo, R. Li, G. Liu, M. R. Antonio and X. Chen, Evidence of trivalent europium incorporated in anatase TiO_2 nanocrystals with multiple sites, *J. Phys. Chem. C*, 2008, **112** (28), 10370-10377.
16. (a) R. L. Penn and J. F. Banfield, Imperfect oriented attachment: dislocation generation in defect-free nanocrystals, *Science*, 1998, **281** (5379), 969-971; (b) J. F. Banfield, S. A. Welch, H. Zhang, T. T. Ebert and R. L. Penn, Aggregation-based crystal growth and microstructure development in natural iron oxyhydroxide biomineralization products, *Science,* 2000, **289** (5480), 751-754.
17. X. Chen, W. Xu, Y. Zhu, P. Zhou, S. Cui, L. Tao, L. Xu and H. Song, Nd_2O_3/Au nanocomposites: Upconversion Broadband Emission and Enhancement under Near-infrared Light Excitation, *J. Mater. Chem. C,* 2014, **2**, 5857-5863.

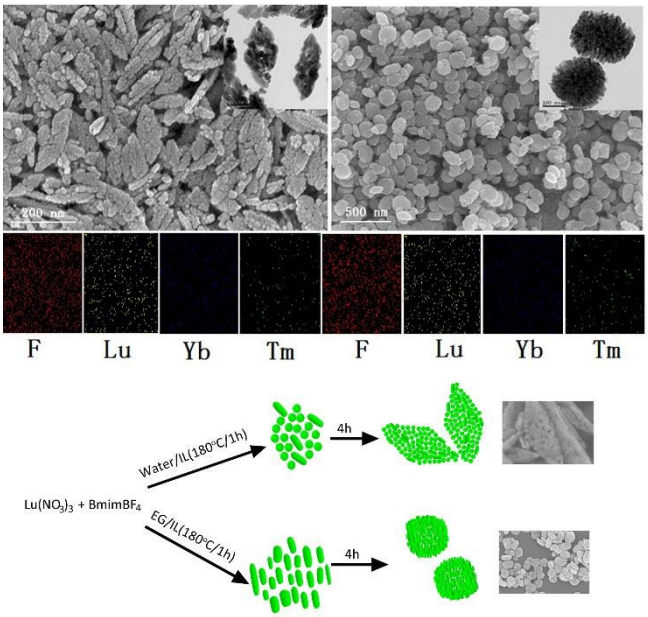

Up-conversion (UC) crystals lanthanide-doped LuF_3 with different morphologies (nanoparticles, shuttle and litchi-like microcrystals) have been synthesized via a facile ionothermal method. The dependence of the diverse morphologies, size and dimensions of the products on the solvent composition and reaction time has been studied in detail, and a possible formation mechanism has also been proposed. The emission spectra showed that the UC luminescence intensity can be adjusted with changing the morphology of LuF_3. Both LuF_3:Yb^{3+}/Er^{3+} and LuF_3:Yb^{3+}/Ho^{3+} nanoparticles synthesized using water/IL (ionic liquid) as mixed solvent exhibit a significant enhancement of the yellowish-green emission under 980nm laser excitation. Besides, nearly NIR (near-infrared) to NIR UC luminescence has been achieved in LuF_3:Yb^{3+}/Tm^{3+} nanoparticles synthesized using EG (ethylene glycol)/IL as mixed solvent. Furthermore, the ratio of the emission intensity of 812nm to that of 545nm reaches 55. Our results indicate that lanthanide-doped LuF_3 provide a promising application in chromatic displays and bio-imaging.